NeuroImage 321 (2025) 121541

Contents lists available at ScienceDirect

NeuroImage

journal homepage: www.elsevier.com/locate/ynimg

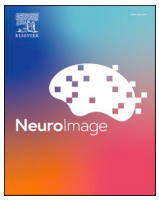

ERP-based interbrain causal model reveals closed-loop information interaction in interpersonal negotiations

Yuqin Li [a], Genon Sarah [b,c], Chunli Chen [a], Lin Jiang [a], Baodan Chen [a], Rihui Li [d], Zhen Liang [e], Jing Yu [f], Debo Dong [b,f], Fen Wan [g], Benjamin Becker [h], Dezhong Yao [a,i,j,*], Fali Li [a,i,k,l,*], Dandan Zhang [m,*], Peng Xu [a,i,n,o,*]

[a] The Clinical Hospital of Chengdu Brain Science Institute, MOE Key Lab for Neuroinformation, School of Life Science and Technology, University of Electronic Science and Technology of China, Chengdu 611731, China
[b] Institute of Neuroscience and Medicine, Brain and Behavior (INM-7), Research Center Jülich, Jülich, Germany
[c] Institute for Systems Neuroscience, Medical Faculty, Heinrich-Heine University Düsseldorf, Düsseldorf, Germany
[d] Center for Cognitive and Brain Sciences, Institute of Collaborative Innovation, University of Macau, Macau S.A.R. 999078, China
[e] School of Biomedical Engineering, Medical School, Guangdong Provincial Key Laboratory of Biomedical Measurements and Ultrasound Imaging, Shenzhen University, Shenzhen 518060, China
[f] Faculty of Psychology, Southwest University, Chongqing 400715, China
[g] Department of Electrical and Computer Engineering, Faculty of Science and Technology, University of Macau, Macau S.A.R. 999078, China
[h] Department of Psychology, and, State Key Laboratory for Brain and Cognitive Sciences, The University of Hong Kong, Hong Kong 999077, China
[i] Research Unit of NeuroInformation, Chinese Academy of Medical Sciences, 2019RU035, Chengdu, China
[j] School of Electrical Engineering, Zhengzhou University, Zhengzhou 450001, China
[k] Department of Radiology, Sichuan Provincial People's Hospital, University of Electronic Science and Technology of China, Chengdu 610072, China
[l] Chinese Academy of Sciences Sichuan Translational Medicine Research Hospital, Chengdu 610072, China
[m] Institute of Brain and Psychological Sciences, Sichuan Normal University, Chengdu 610066, China
[n] Radiation Oncology Key Laboratory of Sichuan Province, Chengdu 610041, China
[o] School of Computer Science and Technology, Southwest University of Science and Technology, Mianyang, 621010, China

ARTICLE INFO

Keywords:
Interbrain couplings
Ultimatum game
Interpersonal negotiations
Event-related potential
EEG hyperscanning

ABSTRACT

Uncovering the interbrain neural mechanisms underlying interpersonal negotiation offers insight into social decision-making dynamics in resource allocation. In this study, we used EEG hyperscanning alongside an iterated ultimatum game to investigate interbrain coupling and dyadic exchange behavior during negotiation. Frontal cortex event-related potentials (ERPs) revealed the distinct neural responses driven by partners' behavioral cues: the proposer's N200 differed significantly for fair versus unfair offers, and the responder's feedback-related negativity (FRN) showed a trend toward significance for the same contrast, while the proposer's N500 varied between acceptance and rejection feedback. Our analysis introduced a novel causal model based on directional phase transfer entropy (dPTE) and time-varying ERP amplitudes, illustrating directed neural processes driven by social exchange, where the proposer's brain activity initially exerts a causal impact on the responder's, whose feedback in turn influences the proposer, creating a closed-loop interaction that drives adaptive negotiation strategies. Additionally, our prediction model with autoregression with exogenous input, which incorporated these causal links between brains, demonstrated higher accuracy than single-brain or reverse causal models, underscoring the significance of dynamic interbrain coupling in interpersonal coordination. This causal model provides a mechanistic explanation of how proposer-responder pairs perceive and adapt to each other's decisions, facilitating shared attention and behavioral coordination in reciprocal, asymmetric negotiations. These findings offer a novel theoretical framework for studying complex social behaviors through interbrain dynamics and may inspire future applications in enhancing cooperative decision-making processes.

* Corresponding authors at: No. 2006, Xiyuan Ave, West Hi-Tech Zone, Chengdu, 611731, Sichuan, China.
E-mail addresses: dyao@uestc.edu.cn (D. Yao), fali.li@uestc.edu.cn (F. Li), zhangdd05@gmail.com (D. Zhang), xupeng@uestc.edu.cn (P. Xu).

https://doi.org/10.1016/j.neuroimage.2025.121541
Received 25 February 2025; Received in revised form 3 August 2025; Accepted 16 October 2025
Available online 17 October 2025

1. Introduction

Interpersonal negotiation—a pervasive aspect of social life—requires constant decision-making to maximize gains and minimize losses. The iterated ultimatum game (UG) is a widely used paradigm for investigating the dynamics of negotiation (Alós-Ferrer et al., 2022; Heffner and FeldmanHall, 2022; Rand et al., 2013). In the UG, a proposer suggests how to split a sum, and the responder chooses to accept or reject the offer. Acceptance results in both parties receiving the proposed amounts; rejection leaves both with nothing. This iterative negotiation creates an asymmetrical, dynamic interaction where roles adapt continually, fostering complementary behaviors. We propose that interacting individuals exhibit a dynamic, non-symmetric coupling rather than simple synchronization, driven by ongoing social exchange. Given the complexities of measuring such coupling, the present study aims to examine brains integration during interactive negotiation by examining interbrain causal coupling (i.e., the directional influence of one individual's brain activity on another's, mediated by shared social context or behavior) via EEG hyperscanning and decoding techniques.

Recent research has shown that interbrain coupling (i.e., neural processes in one brain are coupled to those in another via information exchange during social interaction), such as interbrain synchronization, shapes individual behaviors in social interactions and supports complex social functions (Ma and Tan, 2023; Ni et al., 2024; Pan et al., 2023; Yang et al., 2020; Zhang et al., 2023). Although social behaviors do not directly influence each other's brains, they generate interbrain associations. Identifying neural mechanisms that enable individuals to negotiate could significantly inform models of social interaction. EEG hyperscanning offers a powerful tool to simultaneously monitor the neural activity of interacting participants (Jahng et al., 2017; Kayhan et al., 2022; Szymanski et al., 2017). Foundational studies demonstrate that interacting animals and humans show interbrain EEG synchronizations that encode both self- and partner-related behaviors, predicting future interactions (Gonzalez et al., 2024; Kingsbury et al., 2019). However, existing studies primarily address correlational rather than causal coupling mechanisms in social decision-making (Jiang et al., 2015; Yang et al., 2020). Distinguishing causal from correlative interbrain synchrony is essential, as social stimuli may produce pseudo-correlations in the absence of genuine causal influence (Redcay and Schilbach, 2019; Valencia and Froese, 2020). The causal analysis also clarifies the direction of shared brain states and the behavioral impacts between roles in interactive contexts (Bilek et al., 2022).

Our hypothesis is that directional brain coupling will be present, especially from proposer to responder, reflecting the asymmetrical nature of the UG, where the proposer initiates information flow. We applied directional phase transfer entropy (dPTE) (Hillebrand et al., 2016), a recently introduced, sensitive, computationally efficient, data-driven method for quantifying the intensity and directionality of interpersonal influence during interaction.

Moreover, most previous studies on interbrain causality have primarily derived directed couplings from continuous brain signals (Leong et al., 2017; Schippers et al., 2010). However, neural influences between brains during social interaction are often elicited by behaviorally salient events, which can be effectively captured by time-locked event-related potentials (ERPs). ERPs thus provide crucial insights into real-time interbrain coupling during interactive decision-making (Chuang et al., 2024; Zhang et al., 2019), due to their high temporal resolution and sensitivity to transient neural responses. In fact, the temporal resolution of ERPs could even be superior to EEG oscillations, since ERPs are instantaneous neural responses to events, while EEG oscillations reflect ongoing brain states and connectivity dynamics (Amodio et al., 2014; Pfurtscheller and Lopes da Silva, 1999; Yi et al., 2022). Therefore, ERP-based causal analysis may offer a more precise approach for identifying task-specific interbrain couplings in dynamic interpersonal contexts. In this study, we focused on ERP components extracted from three critical stages of the UG: the proposal, response, and feedback phases. Specifically, we analyzed ERP components such as the N200, feedback-related negativity (FRN), and N500, which are especially relevant to decision-making processes (Gehring and Willoughby, 2002; Hassall et al., 2019; Nieuwenhuis et al., 2004; Polezzi et al., 2008b). The N200, typically occurs approximately 180–280 ms after stimulus onset, is sensitive to high-conflict contexts and strategic adjustments (Clayson and Larson, 2013; Larson et al., 2014). The FRN is commonly elicited by negative feedback, particularly in loss scenarios (Gehring and Willoughby, 2002), involving the medial prefrontal cortex (mPFC) (Cohen et al., 2007; Zhang et al., 2022). It reflects not only whether decision outcomes meet personal expectations but also whether they align with social norms (Miraghaie et al., 2022). The N500 reflects outcome predictability and tends to be larger in response to unpleasant or unpredictable feedback compared to pleasant or predictable outcomes (Mesrobian et al., 2018; Polezzi et al., 2008a, 2008b).

In summary, this study leverages recent EEG hyperscanning advances to reveal interbrain causal mechanisms in dyadic negotiation. First, behavior interactions during iterative UG were assessed, with experimental setups illustrated in Fig. 1. Second, we examined ERP amplitude differences across UG phases (proposal, response, feedback) and scenarios (fair/unfair, accept/reject). More importantly, an interbrain causal model was constructed based on time-variant ERP amplitudes across negotiation stages. Finally, an autoregressive model with exogenous inputs (ARX) was employed to construct both cross-brain causal prediction models and single-brain prediction models, followed by a comparison of their predictive performances. We hypothesize that cross-brain causal prediction models will outperform single-brain models in accuracy, as supported by previous studies (Bilek et al., 2022). This study seeks to uncover the dynamic behavioral interactions and interbrain causal couplings that underpin interpersonal negotiation.

2. Materials and methods

2.1. Participants

In this study, 70 proposer-responder pairs were recruited from the student population of UESTC, totaling 140 right-handed healthy participants (82 males, aged 17–28 years, mean 21.25 years; 58 females, aged 18–26 years, mean 21.87 years). Each pair consisted of two strangers randomly assigned to the roles of proposer and responder. While such pairs are commonly referred to as "dyads" in the hyperscanning and social neuroscience literature (Li et al., 2021; Pan et al., 2023; Pick et al., 2024), we adopt the term "proposer–responder pairs" to emphasize their role-specific interaction within the structured negotiation task and to improve clarity for readers who may be unfamiliar with this domain-specific terminology. All participants had normal or corrected-to-normal vision, no color-vision deficiency, no history of neurological disorders, and no current psychiatric diagnoses or psychotropic prescriptions. Written informed consent was obtained from all participants before their enrollment in the study. The experimental procedures have been approved by the Institution Research Ethics Board of the University of Electronic Science and Technology of China (ApprovalID:1061,423,091,127,369). To evaluate the adequacy of our sample size, a post hoc power analysis was conducted using G*Power 3.1 (Faul et al., 2007). For two-tailed paired samples *t*-tests (Cohen's $d = 0.5$, $\alpha = 0.05$, power $= 0.80$), the required sample size was 34 participant pairs. For correlation analyses ($r = 0.33$, $\alpha = 0.05$, power $= 0.80$), the required sample size was 67 pairs. Thus, our actual sample of 70 pairs of participants exceeds both thresholds and ensures adequate statistical power for the reported analyses.

2.2. Experimental design

The iterated UG is a typical dyadic negotiation scenario that can be employed to investigate physiological correlates of interactive decision-making (Gabay et al., 2014; Yamagishi et al., 2012). Paired participants

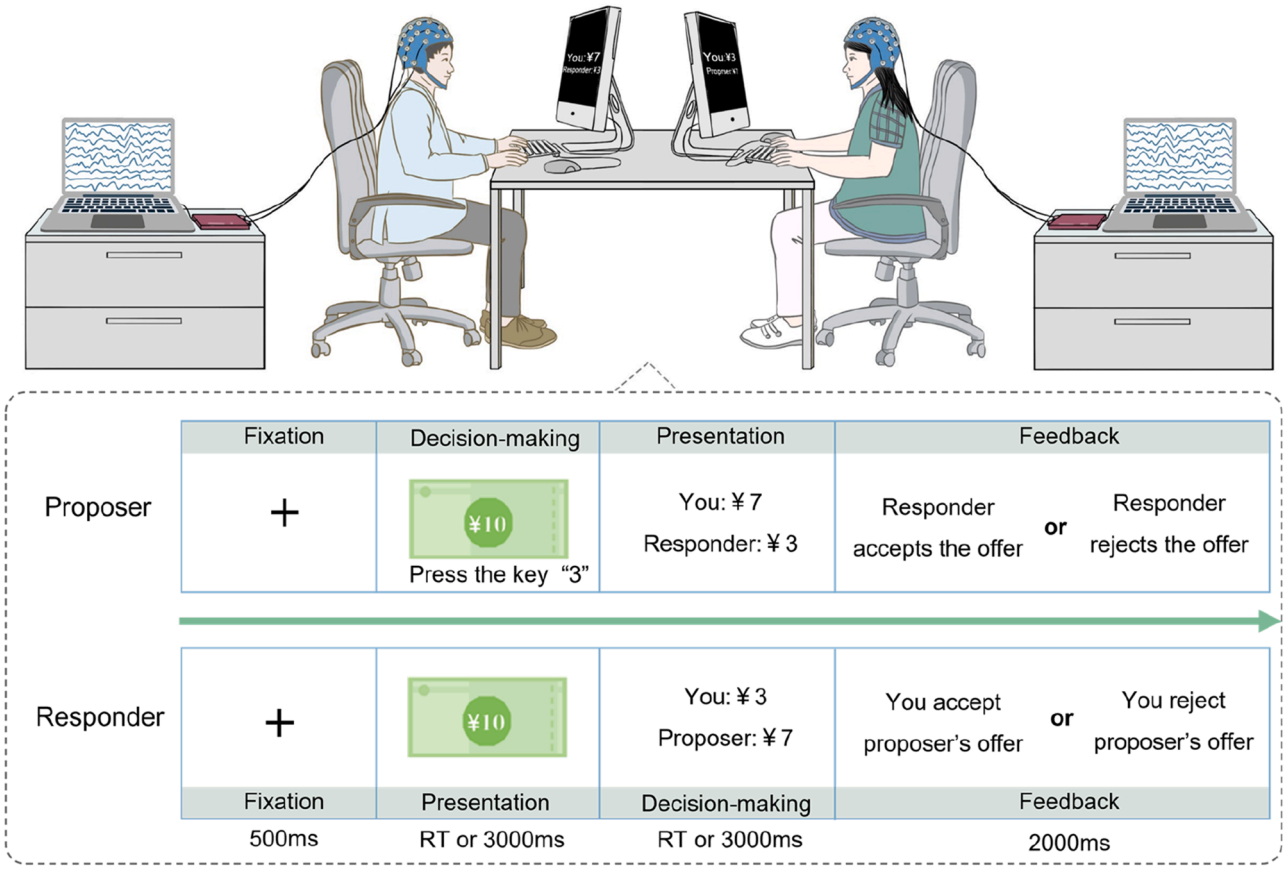

Fig. 1. Experimental setup of the ultimatum game (UG). Experimental design describing the interactive decision-making based on the UG task. Both participants completed the tasks on two back-to-back computers, on which the results of the experiment were presented. The dotted box indicates a representative trial of the UG task. Proposers first gave an offer to responders by selecting one of several valid options via keyboard (e.g., pressing "3″ represents an offer split of 7 vs. 3; valid keys include "1″, "3″, or "5"). Responders then decided to reject or accept the offer. RT represents the response time.

are presented with offers to divide a sum of money with their partners. The proposer determines how to split a specific amount, while the responder decides whether to accept or reject this division. If accepted, both participants receive the specified amount; if rejected, neither participant receives anything. Both participants completed the tasks on two back-to-back computers (Fig. 1), on which the results of the experiment were presented. Throughout the entire task, participants were instructed to keep their gaze fixed on their own screens, minimizing visual contact and non-verbal communication. Notably, the game was played with strangers. Before the experiment, participants were informed about the task and instructed to maximize benefits, with two participants randomly assigned fixed roles. Participants performed the UG task for about 10 min, and EEG data were recorded simultaneously.

The timeline of the tasks is shown in Fig. 1. During the experiment, all stimuli were centrally presented on a computer screen, and responders received a total of 90 offers from the proposer. In each trial, the proposer splits ¥ 10; there are three allocation schemes: the fair (5: 5) and the unfair offers, which consisted of extremely (1: 9) and moderately unfair (3: 7) offers. Each trial started with a 500 ms presentation of a fixation crosshair. Then, a presentation of the total amount allocated was presented on both computer screens. The proposer was required to press the number key (1 for "proposer get ¥ 9, and responder gets ¥ 1″; 3 for "proposer get ¥ 7, responder get ¥ 3″; 5 for "proposer get ¥ 5, responder get ¥ 5") on the keyboard and then the proposed offer was presented on both computer screens. The responders were required to consider the proposal and press a key (2 for "accept'' and 4 for "reject'') to respond. Subsequently, participants would receive the responder's response on the feedback screen (lasting 2000 ms). Following a 2000 ms black screen, the next trial was initiated. In particular, as a proposer or a responder during each trial, the reaction time of the decision should not exceed 3 s, otherwise, there is no gain for each. The participant was given a 30-second break after every 30 trials (30 trials as one block, and the experiment consists of 3 blocks in total).

To accurately assess the cognitive and psychological processes of participants in the UG task, we also collected the interpersonal trust scale (*ITS*) (Rotter, 1967) and the self-report altruism scale (*SAS*) (Gouveia et al., 2010) of all participants prior to the task. Upon completion of the task, participants were asked to complete the same scales once more, with the questions reordered to minimize response bias. Finally, participants were informed of the cumulative bonus and paid out.

2.3. Dual-EEG acquisition

Both participants were comfortably seated in an electrically shielded, sound- and light-attenuated room. Two separate 64-channel ASA-Lab amplifiers (ANT Neuro) with a sampling rate of 500 Hz were used to collect EEG from proposers and responders, respectively. These two acquisition systems received triggers from a server computer's parallel port to ensure signal synchronization. Two electrode caps were positioned following the 10–10 system. During recording, CPz and AFz electrodes served as the reference and ground, respectively. Vertical and horizontal electrooculograms (EOGs) to monitor eye movements were recorded from 2 additional channels located at the right side of the right eye and below the left eye. The online filter band was set at 0.3 ~ 100 Hz. Throughout the tasks, electrode impedances were kept below 5 kΩ, and participants received consistent instructions to relax and minimize

eye movement as well as head or body motion.

2.4. Scale and behavioral analysis

First, for the normal distribution case, two-tailed paired sample *t*-tests were used to quantify potential differences on scales (i.e., *ITS* and *SAS*) between pre- and post-experiment for both the proposer and responder. Decision-making behavioral performance was evaluated using three indices: (a) fair offer rate: percentage of fair offers made by the proposer, (b) acceptance rate: percentage of acceptance feedback made by the responder, and (c) cumulative revenue: cumulative benefits of the proposer. Subsequently, to describe the dynamic behaviors of the proposer and responder at different stages of the UG task, the proposer's time-varying fair offer rate, the responder's time-varying acceptance rate, and the proposer's time-varying cumulative revenue were calculated by adopting the sliding-window strategy. Here, we adopted a 10-trial-length sliding window with an overlapping of 90 % between two adjacency segments, which provided a 1-trial-length temporal resolution. Meanwhile, Pearson's correlation coefficients between pairwise time-varying behavioral series were calculated. Furthermore, to elucidate the relationships of behavioral performances between the two participants, prediction models were constructed based on the responder's acceptance rate, aiming to predict the task behaviors of the proposer (details provided in the SI Appendix). Finally, the potential relationship between scale and behaviors was also explored.

2.5. Dual-EEG analysis

In this study, we exclusively analyzed the task-specific EEG datasets. The analytical procedures consisted of EEG preprocessing, data segmentation, time-frequency analysis, EPR extraction, ERP components determination, time-varying ERP amplitude extraction, interbrain causal model construction based on dPTE, and ERP prediction based on ARX model, as shown in Fig. 2. The details are described below.

2.5.1. EEG preprocessing

The raw EEG datasets were processed offline using EEGLAB and custom MATLAB (v2014a; MathWorks, Inc., USA) scripts. Independent component analysis (ICA) was first applied to remove artifacts, including blinks, eye movements, heartbeat, and myoelectricity (He

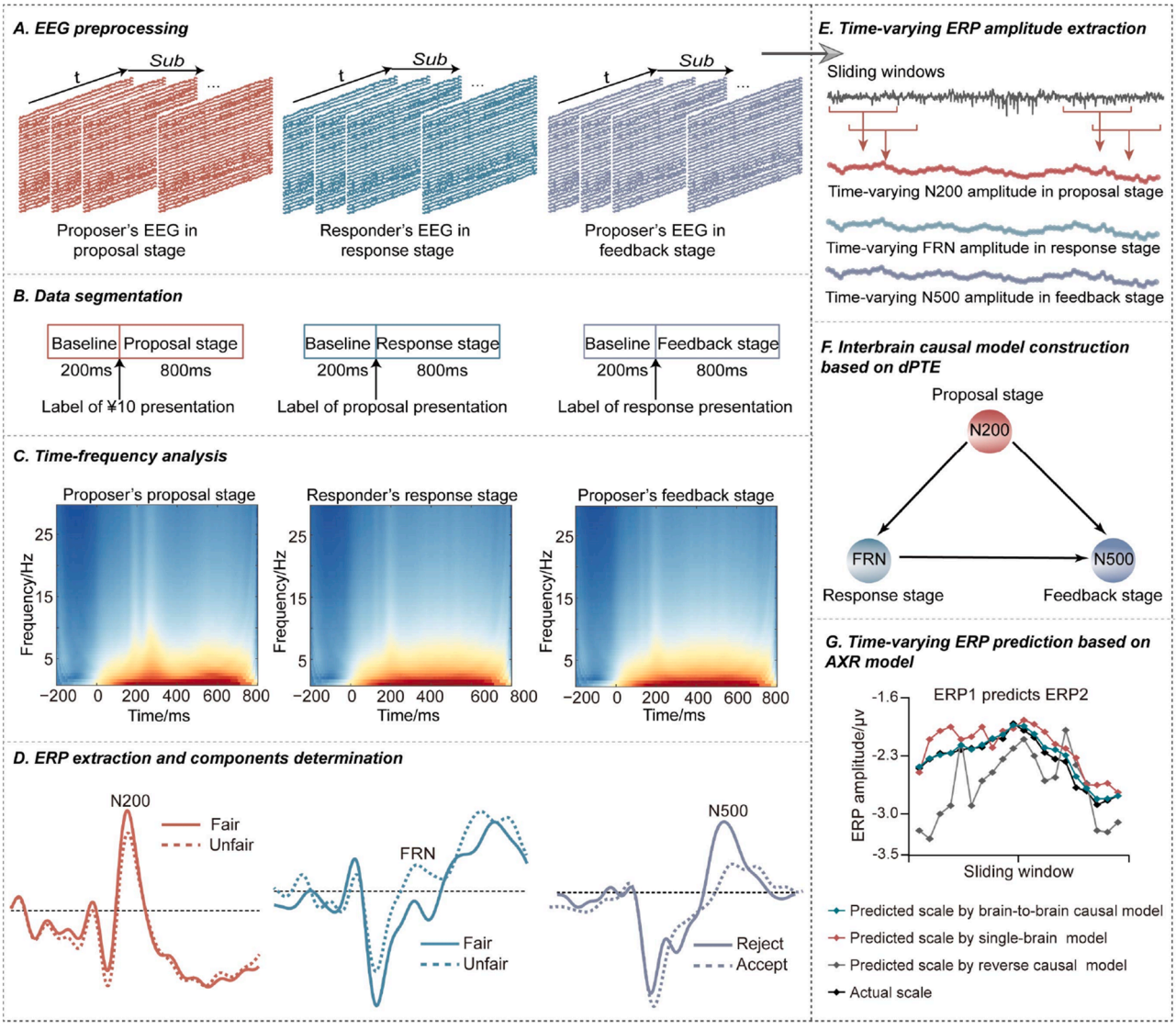

Fig. 2. Analysis procedures for EEG data. (A) EEG preprocessing, (B) EEG data segmentation, (C) Time-frequency analysis to identify the specified response of different frequency bands during the UG task, (D) ERP extraction and ERP components determination, (E) Time-varying ERP amplitude extraction based on the sliding windows, (F) Interbrain causal model construction, and (G) Time-varying ERP prediction based on AXR model. Herein, FRN is the feedback-related negativity, dPTE is the directional phase transfer entropy, and ARX is the autoregression with exogenous input.

et al., 2006), using the Infomax ICA algorithm implemented via the "runica" function in EEGLAB. The identification and removal of artifact components were based on a visual examination of each component's topography, time course, and spectrum, in combination with MARA (Winkler et al., 2011) and IClabel diagnoses (Pion-Tonachini et al., 2019). On average, 1 to 3 artifact components were removed per participant. The EEG data were then re-referenced to a neutral reference using the Reference Electrode Standardization Technique (REST) (Yao, 2001). Thereafter, [1, 30] Hz offline bandpass filtering was applied to the re-referenced data using the "pop_eegfiltnew" function in EEGLAB. For both the proposer and responder, EEG data from the decision and feedback stages were extracted based on event markers corresponding to stimulus onset. Data epochs were segmented into 1-second windows, ranging from 200 ms before to 800 ms after the onset of the visual stimulus (i.e., when the task-relevant screen was presented), as shown in Fig. 2B After identifying target trials (i.e., trials from proposer's proposal stage, responder's response stage, and proposer's feedback stage), baseline correction (baseline from −200 to 0 ms) and artifact-trial removal by a threshold of ±120 μV were applied. Only those epochs without artifacts were considered for further analysis. The proposer's proposal stage included 88.2 ± 2.4 epochs, the responder's response stage included 88.7 ± 2.4 epochs, and the proposer's feedback stage included 87.3 ± 4.1 epochs.

2.5.2. ERP extraction

The frontal cortex plays a critical role in human decision-making, as evidenced by its continuous internal monitoring of decision feedback and processing of high-conflict decision situations (Amodio and Frith, 2006; Paret et al., 2016; Rushworth et al., 2011). Therefore, in this study, frontal ERP is primarily extracted. Before ERP extraction, aiming to investigate the dynamics of task-related brain activity in the frequency domain, we acquired the time-frequency distributions (TFDs) for time sequences from the frontal lobe by using the wavelet toolbox in MATLAB (v2014a). Particularly, we first calculated the TFDs for each artifact-free trial, and the TFDs were then grand-averaged across trials and subjects to achieve mean TFDs for each experimental stage. The results revealed that the task-related time-frequency activities predominantly concentrated on [1 – 10] Hz (Fig. 4A), while higher frequency bands were markedly attenuated. Therefore, we applied an additional 1–10 Hz band-pass filter prior to ERP averaging to emphasize the dominant low-frequency components and enhance the signal-to-noise ratio for visualization and analysis.

Considering consistent findings from numerous studies that proposers make decisions with high conflict, resulting in increased activation in the frontal and central regions (Vallet et al., 2019; Yin et al., 2016), we focused on the N200 component during the proposal stage. Specifically, for each participant, the individual peak latency within 180–280 ms was identified separately at electrodes FCz and Fz. The mean amplitude within ±20 ms around each peak was then calculated for each electrode, and these two values were averaged to obtain the final N200 amplitude. N200 amplitudes under fair and unfair conditions were then compared using two-tailed paired *t*-tests. Inspired by previous research (Billeke et al., 2013; Polezzi et al., 2008b), we examined the FRN and N500 components at electrode Fz during the response and feedback stages. For the response phase, FRN amplitudes were extracted by identifying individual peaks within 220–350 ms and calculating mean amplitudes within ±20 ms, under both fair and unfair conditions, followed by two-tailed paired samples *t*-tests. During the feedback stage, FRN (220–350 ms) and N500 (400–600 ms) amplitudes were similarly extracted after proposal acceptance or rejection and compared using two-tailed paired samples *t*-tests. All electrode selections and time windows were informed by prior literature and visually confirmed in grand-averaged waveforms. The details of the amplitude of the ERP components extracted are reported in the SI Appendix.

2.5.3. Estimation of preferential causality based on dPTE

To further investigate the interbrain causal coupling, the dPTE (Hillebrand et al., 2016) was wielded to estimate the preferential causality of two time-varying ERP amplitude sequences derived from the proposer and responder. The range of dPTE values is from 0 to 1, with a threshold of 0.5 indicating no preferential direction of information flow. If information flows from time series *i* to time series *j*, then $1 > \mathrm{dPTE}_{i,j} > 0.5$; conversely, $0 < \mathrm{dPTE}_{i,j} < 0.5$ holds for opposite directionality. Specifically, to obtain time-varying ERP amplitude sequences, we applied a 10-trial-length sliding window across the 90 trials. Each window included 10 consecutive trials, and adjacent windows overlapped by 90 %, resulting in a total of 81 sliding windows. For each window, EEG epochs were averaged to obtain a mini-ERP, from which the N200, FRN, and N500 amplitudes were extracted as described above. If any trials within a given window contained artifacts, they were excluded before averaging. This procedure generated time-varying ERP amplitude sequences. Subsequently, dPTE was calculated between the ERP amplitude sequences from the two participants in each proposer-responder pair. The final causality value was obtained by averaging the dPTE values across all pairs. Detailed methods for dPTE are provided in the SI Appendix.

Thereafter, permutation testing (1000 times) was used to determine whether the observed (original) dPTE explained the pattern of information flow between two time-varying amplitude sequences better than would be expected by chance. Concretely, for the causal information flow between two time-varying ERP amplitudes, the statistical significance was assessed by a non-parametric permutation test. In each permutation test, the time-varying N200/FRN/N500 amplitudes were shuffled randomly, and the entire calculation process of dPTE was performed to obtain a dPTE_perm based on the shuffled dataset. This procedure was repeated 1000 times, and the final p-value was calculated as the proportion of permutations where the absolute deviation of dPTE_perm from 0.5 was equal to or greater than that of the original dPTE. This two-tailed permutation test allows detection of significant directed information flow in either direction.

2.5.4. Autoregression with exogenous input model for ERP prediction

The ARX model has been widely employed for signal prediction (Jiang et al., 2019). In this study, the improved ARX model was used to describe the time-varying ERP interactions of the proposer and responder. Specifically, the N200 amplitude sequence (i.e., input) of the proposer was used to predict the FRN amplitude sequence (i.e., output) of the responder, and the latter was subsequently employed to predict the N500 amplitude sequence (i.e., output) during feedback from the proposer. To avoid the influence of a participant's own past ERP amplitude series on the ARX prediction model, we used only the single participant's own past amplitude data and the reverse cross-brain model for prediction, and then compared their predictive performance. Importantly, to quantitatively index the performance of the predicting model, the Pearson's correlation coefficients between all participants' actual and predicted amplitude under each sliding window, as well as between all windows' actual and predicted amplitude for each participant, together with root mean square error (*RMSE*), were calculated. Further details regarding ARX can be found in the SI Appendix.

3. Results

3.1. Scale and individual behaviors

First, the changes in the interpersonal interaction-related scales (i.e., *ITS* and *SAS*) before and after conducting the UG experiments were probed. Two-tailed paired sample *t*-tests revealed significant differences in both *ITS* and *SAS* scores between pre- and post-task. For proposers, post-task scores were significantly higher than pre-task scores for *ITS* (mean change = +4.7 ± 1.2, $t = 4.072$, $p < 0.001$) and *SAS* (mean change = +0.34±0.15, $t = 2.274$, $p = 0.026$). Similarly, responders also

showed significant increases in *ITS* (mean change = +3.0 ± 1.1, t = 2.684, p = 0.009) and *SAS* (mean change = +0.25 ± 0.12, t = 2.096, p = 0.040), as shown in Fig. 3A. Second, the time-varying fair offer rate (tFO) of the proposer, time-varying acceptance rate (tAR) of the responder, and the time-varying cumulative revenue (tCR) of the proposer were calculated. To quantitatively describe the changing trend of the behaviors, the linear fitting slope of each participant's time-varying behavior was calculated. By conducting the one-tailed hypothesis test against zero for the slope, a gradual increase in tFO (t = 1.918, p = 0.030, showing a trend toward significance) of the proposer, tAR (t = 2.244, p = 0.014) of the responder, and tCR (t = 2.244, p = 0.014) of the proposer were observed (see Fig. 3B). Furthermore, positive correlations among these behaviors were found using Pearson's correlation and predictive analysis. Detailed information was summarized in the SI Appendix, Figs. S1A-B. Third, the associations between differences in scales (i.e., *ITS* and *SAS*) and fluctuations in behavior before and after the task were examined, with multiple correlations corrected using the false discovery rate (FDR). As presented in Fig. 3C, the fluctuations of the proposer's cumulative revenue (r = 0.343, p_{FDR} = 0.004) were positively correlated with their own *ITS* difference, and the fluctuations of the proposer's fair offer rate (r = 0.333, p_{FDR} = 0.006) were positively related to the responder's *ITS* difference. The correlation coefficient r and the statistical significance level p between the scale differences and the behavioral fluctuations as shown in Table S1.

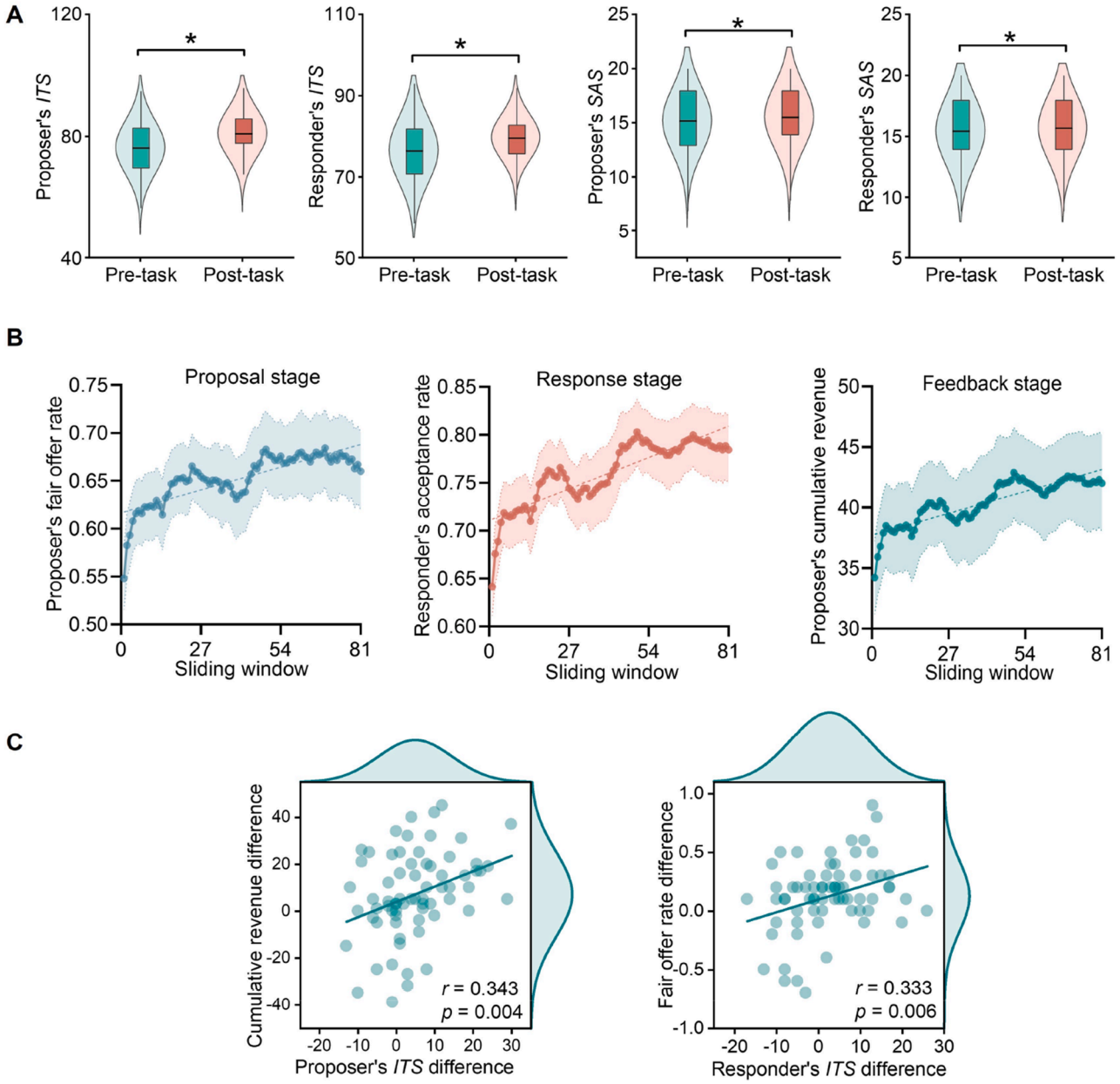

Fig. 3. Scale and behavior results. (A) Interpersonal trust scale (*ITS*) and self-report altruism scale (*SAS*) scores of the proposer and responder before and after tasks. Asterisk indicates statistically significant difference ($p < 0.05$, two-tailed). (B) Temporal dynamics of proposer's fair offer rate, responder's acceptance rate, and proposer's cumulative revenue during the UG. In each subfigure, values are the mean and standard error (mean ± *s.e.*) of time-varying behaviors. One-tailed t-tests against zero were used to assess the significance of increasing trends over time ($p < 0.025$). (C) Relationships between scale differences and behavioral fluctuations. In each subfigure, the distribution of behaviors and scales is shown on the right and upper sides of the frame, respectively; the green line is the fitted curve, r is the correlation coefficient, and p represents the statistical significance level.

3.2. Grand-mean ERP statistics

The temporal dynamics of three ERP components (i.e., N200, FRN, and N500) were explored in this study to unravel the development of interpersonal interaction over time (Du et al., 2022). To investigate the specified response of different frequency bands and time points during the UG task, TFDs for both participants were initially calculated. Fig. 4A shows the averaged TFDs on the frontal lobe. In specific, it was determined that brain activity during tasks was mainly concentrated in the 1∼10 Hz frequency range; by contrast, the high band activity is attenuated. Thus, a 1∼10 Hz bandpass filter was applied to extract ERPs accordingly. The filter was implemented using a zero-phase sinc finite impulse response (FIR) filter with an order of 200 and a Hamming window, applied via the "pop_eegfiltnew" function in EEGLAB. According to the results and previous research on decision-making (Gehring and Willoughby, 2002; Hassall et al., 2019; Nieuwenhuis et al., 2004; Polezzi et al., 2008b), this study mainly focused on the N200, FRN, and N500 to investigate the ongoing interbrain interactions during their participation in the UG tasks.

First, the N200 from the proposers was extracted during the proposal

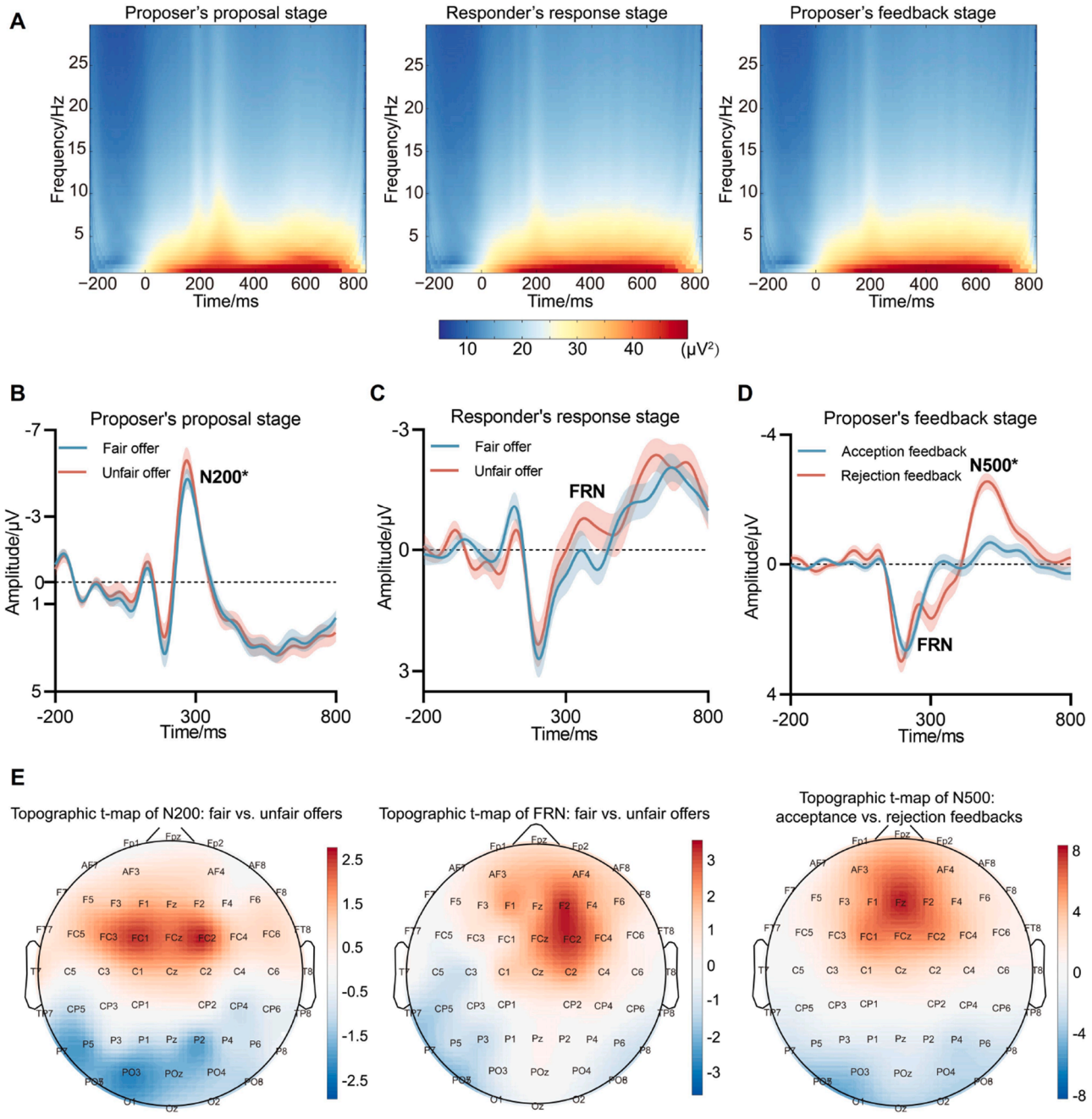

Fig. 4. Grand-mean ERP results. (A) Time-frequency distributions of the frontal lobe for the proposer's proposal stage, responder's response stage, and proposer's feedback stage. (B) The ERP waveforms under fair and unfair conditions for the proposers at the proposal stage. (C) The ERP waveforms under fair and unfair conditions for the responders at the response stage. (D) The ERP waveforms under acceptance and rejection feedback for the proposer at the feedback stage. The blue and red lines (shadows) indicate the mean (s.e.) of the fair (acceptance) and unfair (rejection) ERP in all subjects, respectively. Asterisk indicates statistically significant difference ($p < 0.05$, two-tailed). (E) The topographic t-maps of both conditions (e.g., fair offer vs. unfair offer, and acceptance feedback vs. rejection feedback). Higher t-values indicate greater differences, primarily localized in frontal regions. Warmer colors (e.g., red) indicate greater amplitudes for unfair offers (N200, FRN) or rejection feedback (N500), while cooler colors (e.g., blue) indicate the opposite. Color bar represents t-values (unitless).

stage. A two-tailed paired-samples *t*-test revealed a significant difference in N200 amplitudes between unfair and fair proposals ($p = 0.019$), with unfair proposals evoking larger amplitudes (-5.312 ± 0.669 μV; mean ± *s*.e.) than fair proposals (-4.481 ± 0.521 μV) at electrodes FCz and Fz (see Fig. 4B). A two-tailed paired-samples *t*-test revealed no statistically significant difference in FRN amplitudes between unfair and fair proposals ($p = 0.08$) at electrode Fz. However, a trend toward larger FRN amplitudes in response to unfair proposals (-1.266 ± 0.359 μV) compared to fair proposals (-0.673 ± 0.314 μV) was observed. Third, the FRN and N500 amplitudes were extracted during the feedback stage. A two-tailed paired-samples *t*-test revealed a significant difference in N500 amplitudes between rejection and acceptance feedback ($p < 0.001$), with rejection feedback evoking larger amplitudes (-3.328 ± 0.234 μV) than acceptance feedback (-1.305 ± 0.180 μV) at electrode Fz (see Fig. 4D). In contrast, there was no significant difference in FRN amplitudes between acceptance (-0.433 ± 0.200 μV) and rejection (-0.364 ± 0.331 μV) feedback ($p = 0.415$). Therefore, subsequent analyses were performed based on the N200, FRN, and N500 components of the proposal, response, and feedback stages, respectively. Meanwhile, paired samples *t*-tests were conducted to examine topographic differences in the amplitudes of three ERP components (i.e., N200, FRN, and N500) between conditions (e.g., fair vs. unfair offers and acceptance vs. rejection feedback). The resulting t-value topographic maps (Fig. 4E) indicate that significant differences are predominantly localized in the frontal cortex.

3.3. Interbrain causal model of the ERP components

The dPTE was used to assess the preferred direction of information transmission for time-varying ERP amplitudes between proposers and responders. The process of extracting time-varying ERP amplitude sequences for each participant is illustrated in Figs. 5A-C. By definition, a $dPTE_{xy}$ greater than 0.5 indicates that information flows preferentially from time series *X* to time series *Y*; whereas, a $dPTE_{xy}$ smaller than 0.5 indicates that information flows preferentially from time series *Y* to time series *X*. Fig. 5D depicts the preferred direction of information flow. There exists a subtle but significant causal pact of the proposer's N200 amplitude on the responder's FRN amplitude (dPTE = 0.5231,

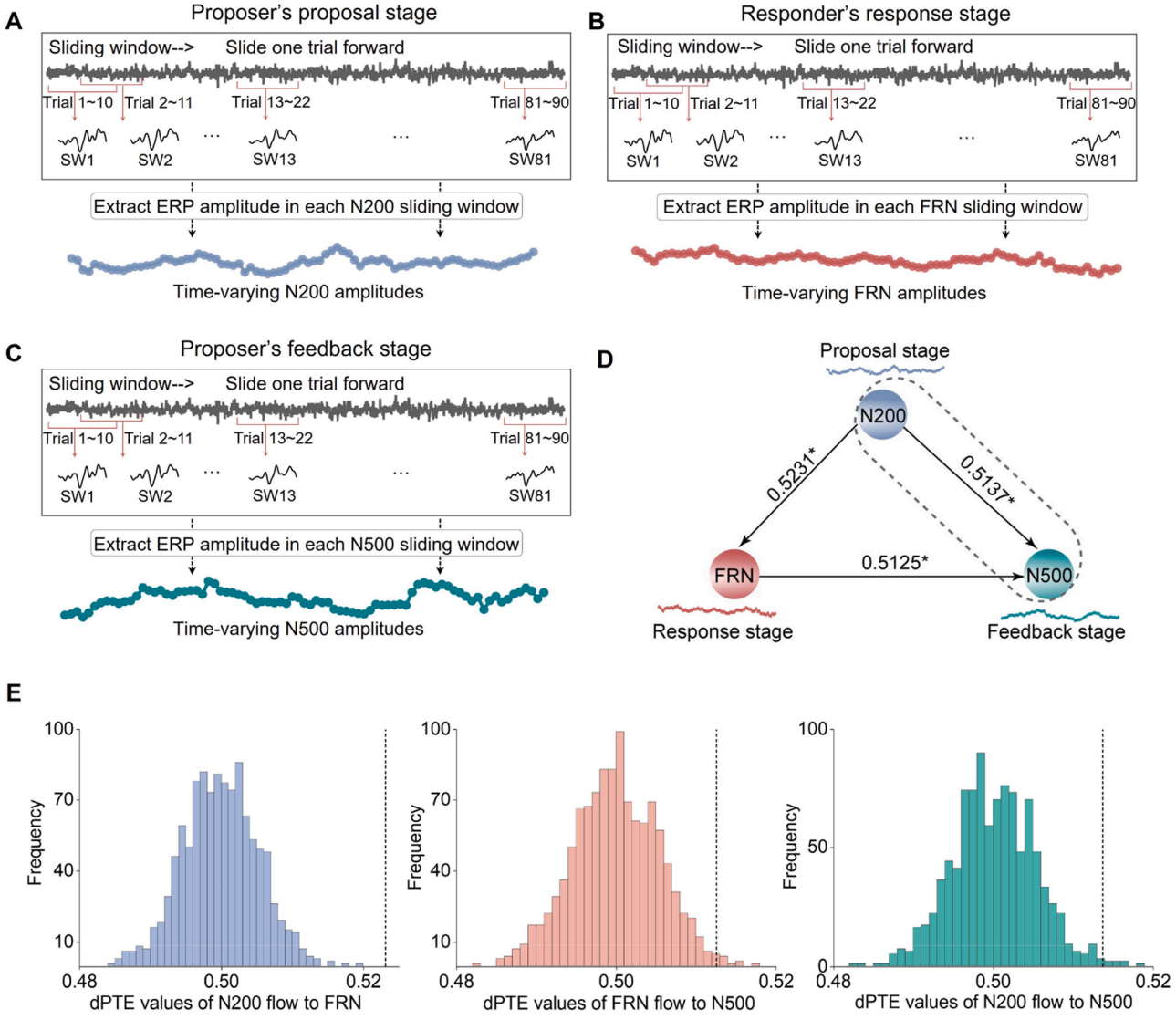

Fig. 5. Interbrain causal model. (A-C) Extraction of the time-varying N200/FRN/N500 amplitude. Using a 10-trial-length sliding window (SW) with an overlapping of 90 % between two adjacent segments, time-varying amplitude sequences of ERP components of the proposer and responder were obtained. (D) Causal model for different time-varying ERP amplitude sequences. The causal flow in the dashed box represents intra-brain coupling, and the causal flow without a box represents interbrain coupling. * indicates $p_{permutation} < 0.05$. (E) Permutation testing results of the dPTE values. After 1000 random shufflings of the time-varying ERP amplitudes, the 1000 dPTE values were obtained. The black dashed lines denote the positions of the actual dPTE values.

$p_{permutation} < 0.001$, two-tailed) and the proposer's N500 amplitude (dPTE = 0.5137, $p_{permutation} = 0.012$, two-tailed). Additionally, in determining the causal relationship between the brain activity of the response and feedback stages, the responder's FRN amplitude showed a significant directional effect on the proposer's N500 amplitude (dPTE = 0.5125, $p_{permutation} = 0.020$, two-tailed). Fig. 5E shows the permutation test results.

Moreover, the relationships between ERP (i.e., N200, FRN, and N500) and behavioral fluctuations (i.e., proposers' fair offer rate, responders' acceptance rate, and proposers' cumulative revenue) were explored and adjusted for multiple correlations using FDR. As shown in Fig. 6, the fluctuations in fair offer rate ($r = 0.348$, $p_{FDR} = 0.004$), acceptance rate ($r = 0.333$, $p_{FDR} = 0.005$), and cumulative revenue ($r = 0.293$, $p_{FDR} = 0.015$) were significantly positively correlated with the fluctuations in N500 amplitude. The correlation coefficient r and the statistical significance level p between the behavior fluctuations and the ERP fluctuations as depicted in Table S2.

3.4. Prediction results based on the interbrain causal relationships

To advance a comprehensive understanding of the functional meaning of interbrain causal couplings during interpersonal negotiations, prediction models were developed using ARX to account for time-varying interbrain flows between the two participants. In the single-brain prediction model, an individual's own time-varying ERP amplitude sequence served as both the input and the target output, thereby modeling the prediction of future neural responses based solely on one's own past activity. In contrast, the causal and reverse causal cross-brain prediction models used the partner's signal as the input and the individual's own signal as the output, enabling the prediction of future neural activity based on both the individual's and their partner's past signals. Fig. 7 depicts the correlation coefficient *R* and *RMSE* between actual and predicted ERP amplitudes predicted for a single subject and for a single sliding window (SW) by the causal cross-brain and single-brain prediction models, respectively, and SI Appendix, Figs. S2–3 depicts the *RMSE* between the actual and predicted ERP amplitudes predicted for a single subject and for a single SW by the reverse causal cross-brain prediction model, respectively.

Specifically, as shown in Figs. 7A-B, two-tailed paired samples *t*-tests revealed that compared to the correlation coefficient *R* (single subject: 0.893 ± 0.007 μV; single SW: 0.949± 0.001 μV) and *RMSE* (single subject: 0.817 ± 0.018 μV; single SW: 0.828 ± 0.008 μV) between actual and predicted FRN amplitudes in the single-brain prediction model, the correlation coefficient *R* (single subject: 0.918 ± 0.005 μV; single SW: 0.960± 0.001 μV, $p < 0.001$) between actual and predicted FRN amplitudes was found to be larger and the *RMSE* (single subject: 0.714 ± 0.16 μV; single SW: 0.724 ± 0.007 μV, $p < 0.001$) was found to be smaller in the causal cross-brain prediction model. Figs. 7C-D illustrates that the correlation coefficient *R* between the actual and predicted N500 amplitudes of the causal cross-brain prediction model (single subject: 0.893 ± 0.006 μV; single SW: 0.935 ± 0.002 μV) were higher than that of the single-brain prediction model (single subject: 0.867 ± 0.007 μV; single SW: 0.920 ± 0.003 μV, $p < 0.001$), while the *RMSE* between the actual and predicted N500 amplitudes of the causal cross-brain prediction model (single subject: 0.721 ± 0.024 μV; single SW: 0.744 ± 0.010 μV) were lower than that of the single-brain prediction model (single subject: 0.809 ± 0.026 μV; single SW: 0.832 ± 0.012 μV, $p < 0.001$). Furthermore, to verify the unique predictive value of the causal cross-brain prediction model, ERP amplitudes were predicted based on the reverse cross-brain causal prediction model. The correlation coefficient *R* of the reverse causal cross-brain prediction model was found to be significantly lower, and the *RMSE* was found to be significantly higher than those of the causal cross-brain and single-brain models. The corresponding results are summarized in the SI Appendix, Figs. S2–3. Therefore, a prediction model that includes causal relationships between the brains of interacting individuals is more effective in predicting performance than prediction models that do not include between-brain and reverse causal relationships, as shown by the significantly larger correlation coefficient *R* and smaller *RMSE* between the actual and predicted ERP amplitudes.

4. Discussion

Understanding the social brain requires a two-person perspective that captures its dynamic adaptations to others during ongoing interactions (Redcay and Schilbach, 2019). However, the interbrain causal mechanisms underlying interpersonal coordination, particularly in asymmetrical decision-making contexts, remain unclear. In this study, we employed EEG hyperscanning to investigate directional influences between the brain activities of interacting individuals during economic negotiation, and to examine interpersonal scales and behavioral changes in participant pairs. The results show three key findings: 1) Reciprocal patterns in interpersonal scales and behaviors, suggesting compromise and cooperative behavior emerging from self-interest during negotiation; 2) Significant ERP differences were found, with larger N200 in proposers and a trend toward larger FRN in responders for unfair offers, and larger N500 in proposers following rejection feedback; and 3) There exists a causal coupling between time-varying ERP amplitudes, enabling effective prediction of the partner's subsequent brain activity. This study is, to our knowledge, the first to investigate ERP-based causal couplings, offering a promising approach for studying complex social behaviors within EEG hyperscanning.

Social bonding is sustained by interactive experiences that shape individual dispositions and internal preferences (Bault et al., 2017). Rotter's trust theory posits that trust is rooted in expectations shaped by social exchanges (Rotter, 1967). The observed increase in interpersonal trust and altruism scores after partner interaction suggests stronger prosocial dispositions (Philippe Rushton et al., 1981; Thielmann et al., 2020; van Dijk and De Dreu, 2021), with significant positive correlations between trust scores and negotiation performance. These results imply

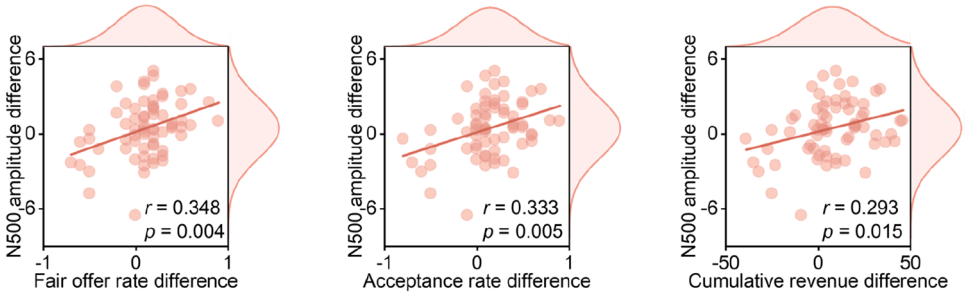

Fig. 6. Relationships between the fluctuations of ERP amplitudes and decision-making behaviors. In each subfigure, the distribution of behaviors and ERP amplitudes is shown on the right and upper sides of the frame, respectively; the red line is the fitted curve, *r* is the correlation coefficient, and *p* represents the statistical significance level.

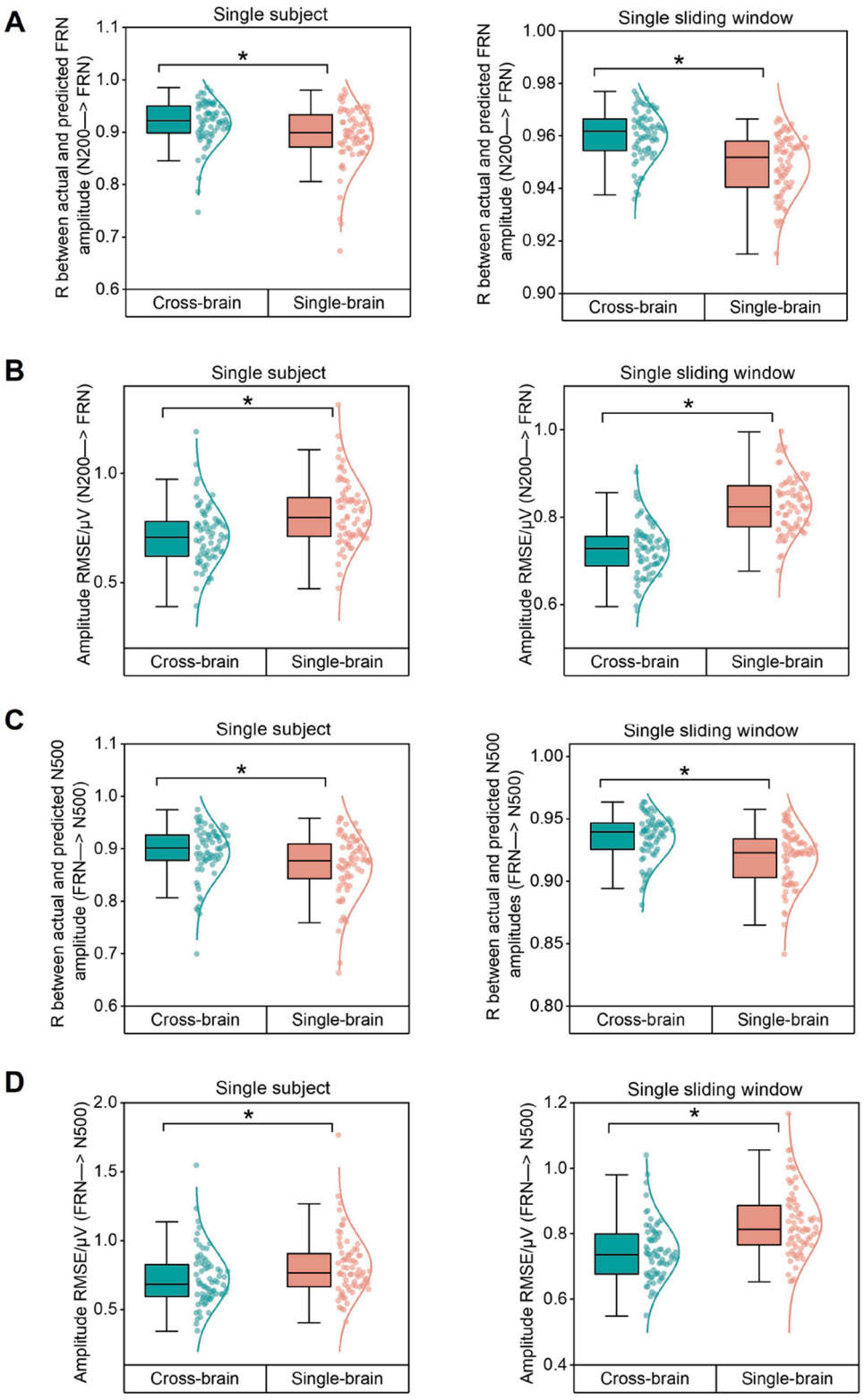

Fig. 7. Prediction results of the ARX model. (A) Correlation coefficient *R* between the actual and predicted amplitudes for the causal cross-brain (N200 predicted FRN) and single-brain (FRN predicted FRN) prediction models in the single subject and the single sliding window. (B) *RMSE* between the actual and predicted amplitudes for the causal cross-brain (N200 predicted FRN) and single-brain (FRN predicted FRN) prediction models in the single subject and the single sliding window. (C) Correlation coefficient *R* between the actual and predicted amplitudes for the causal cross-brain (FRN predicted N500) and single-brain (N500 predicted N500) prediction models in the single subject and the single sliding window. (D) *RMSE* between the actual and predicted amplitudes for the causal cross-brain (FRN predicted N500) and single-brain (N500 predicted N500) prediction models in the single subject and the single sliding window. The *RMSE* is the root mean square error, * represents $p < 0.05$. N200—> FRN and FRN—> N500 represent information flows preferentially from N200 to FRN and information flows preferentially from FRN to N500, respectively.

that reciprocal beliefs are reinforced through repeated social exchanges with unfamiliar partners, fostering trust and prosocial behavior that facilitate cooperative negotiation. Interestingly, despite the post-task increase in self-reported altruism, it did not correlate with behavioral outcomes, suggesting that behavioral change in dynamic negotiation may be more strongly driven by situational trust shaped through ongoing interaction than by altruistic tendencies. This supports the earlier observation of reciprocal patterns in interpersonal scales and behaviors, indicating that cooperation emerges more from mutual adaptation and self-interest negotiation than from generalized prosocial traits. In behavioral terms, using real participants enhances ecological validity over traditional UG paradigms. Responders' tendencies to reject low offers compelled proposers to share more equitably, resulting in balanced outcomes and effective coordination as negotiations progressed. Prior behaviors informed each party's intention, indicating that feedback from responders on earlier proposals shaped proposers' subsequent offers, establishing adaptive and cooperative strategies.

At the neural level, ERP components (N200, FRN, and N500) varied significantly across UG stages and conditions. During the proposal phase, high N200 amplitudes for unfair offers reflected increased conflict processing, consistent with prior findings (König et al., 2021; Whitehead et al., 2017). In the response phase, responders' FRN amplitude showed a trend toward greater negativity for unfair offers, indicating a potential sensitivity to fairness violations (Fehr and Fischbacher, 2003; Mayer et al., 2019). During feedback, rejection feedback elicited a pronounced N500 response, reflecting proposers' heightened sensitivity to negative feedback (Bellebaum et al., 2010; Chen et al., 2010). The N500 component may reflect the cognitive evaluation of outcome expectancy violations and the adjustment of future decision strategies. Significant correlations between N500 fluctuations and behavioral adjustments further indicate that dynamic brain responses are shaped by reciprocal behavioral cues, underscoring the iterative, interactive nature of interpersonal negotiation.

Beyond individual neural changes, accumulating evidence suggests that interbrain correlation is an inherent feature of complex social interactions, primarily facilitating execution and coordination (Hasson et al., 2012; Kingsbury and Hong, 2020; Zhang and Yartsev, 2019). Most studies have examined interbrain synchrony, defined as the temporal alignment of neural activity between social partners (Feldman, 2007; Kingsbury et al., 2019; Valencia and Froese, 2020). However, the iterated UG involves asymmetric proposer-responder roles, making it essential to characterize the directionality of interbrain coupling to better understand dynamic decision-making processes (Bilek et al., 2022). Our findings demonstrate that temporal variations in the brain activity of proposers and responders carry information about their partner's state, reflecting shared attention and mutual adaptation during negotiations. Although emerging research has started to assess the directionality of information flow between brains (Leong et al., 2017; Qiao et al., 2025; Schippers et al., 2010), most have focused on joint attention tasks or non-iterative paradigms. In contrast, by leveraging a novel analytical framework based on time-varying ERP amplitudes and dPTE, we identified interbrain causal coupling: the proposer had a significant influence on responder's neural information during the initial phase, as proposers introduced offers, while the feedback phase closed this loop, with responders' choices guiding proposers' future offers. These findings align with prior work showing that interactive behavioral information, mediated through real-time feedback and non-verbal cues, fosters interbrain coupling within dyadic partners (Jiang et al., 2012; Luft et al., 2022; Speer et al., 2024).

Notably, while the observed dPTE values indicate only modest deviations from 0.5, this pattern is consistent with prior research (Hillebrand et al., 2016) and reflects a statistically reliable directional bias in interactions of neural activities. This directional coupling, although subtle, provides insight into how role-based asymmetries (e.g., proposer *vs*. responder) modulate the temporal evolution of neural information during dynamic social exchange. Like the neural synchrony observed in animal studies (Kingsbury et al., 2019), our ERP-based prediction models demonstrate that including interbrain causal relationships enables more accurate prediction of a partner's brain activity than single-brain models. This model of causal coupling illuminates how interbrain dynamics evolve alongside behavioral negotiation, each informing and refining the other.

In summary, this study identified distinct behavioral interaction patterns and directional interbrain coupling during dyadic economic negotiation. The use of ERP-based causal coupling provides new insights into human behavior in asymmetrical interactive decision-making, with implications for developing interventions targeting ERP-based coupling. For instance, future studies could explore whether neuromodulation (e.g., transcranial magnetic stimulation (TMS)) applied to one partner's brain activity might indirectly influence the other's neural or behavioral responses during interaction, thereby facilitating interpersonal coordination and providing further evidence for directional interbrain influence. Nevertheless, several limitations should be acknowledged. First, although the observed causal effects reached statistical significance, the corresponding effect sizes (dPTE values ~0.51–0.52) were modest. These subtle effects warrant cautious interpretation. Future studies with increased statistical power—through larger samples, improved signal-to-noise ratio, or multimodal imaging—are necessary to validate and extend these findings. Second, although there was a trend for unfair proposals to evoke larger FRN amplitudes compared to fair proposals, this difference did not reach statistical significance in two-tailed tests ($p = 0.08$). This borderline result may reflect limited statistical power or variability in neural responses, warranting further investigation with larger samples. Finally, given the turn-taking, computer-mediated setup of the current paradigm, future studies could adopt more naturalistic, unconstrained interaction settings to capture interbrain causal dynamics more profoundly, enriching our understanding of human social interaction in this most authentic form.

CRediT authorship contribution statement

Yuqin Li: Writing – original draft, Visualization, Software, Methodology, Formal analysis, Data curation, Conceptualization. **Genon Sarah:** Writing – review & editing, Conceptualization. **Chunli Chen:** Methodology, Data curation. **Lin Jiang:** Methodology. **Baodan Chen:** Data curation. **Rihui Li:** Writing – review & editing, Investigation. **Zhen Liang:** Writing – review & editing. **Jing Yu:** Writing – review & editing. **Debo Dong:** Writing – review & editing. **Fen Wan:** Writing – review & editing. **Benjamin Becker:** Writing – review & editing. **Dezhong Yao:** Writing – review & editing, Supervision, Resources. **Fali Li:** Writing – review & editing, Supervision, Investigation, Funding acquisition, Conceptualization. **Dandan Zhang:** Writing – review & editing, Methodology. **Peng Xu:** Writing – review & editing, Supervision, Project administration, Funding acquisition, Conceptualization.

Declaration of competing interest

The authors declare that the research was conducted in the absence of any commercial or financial relationships that could be construed as potential conflicts of interest.

Acknowledgements

This work was supported by the National Natural Science Foundation of China (#W2411084, #82372084), the Key R&D projects of the Science & Technology Department of Chengdu (#2024-YF08–00072-GX), the STI 2030-Major Projects (#2022ZD0208500), and the Sichuan Science and Technology Program (2024NSFTD0032).

Supplementary materials

Supplementary material associated with this article can be found, in

the online version, at doi:10.1016/j.neuroimage.2025.121541.

Data availability

The raw EEG of all subjects and custom routines for data analysis written in MATLAB are available from the corresponding author on reasonable request.

References

Alós-Ferrer, C., García-Segarra, J., Ritschel, A., 2022. Generous with individuals and selfish to the masses. Nat. Hum. Behav. 6, 88–96.

Amodio, D.M., Bartholow, B.D., Ito, T.A., 2014. Tracking the dynamics of the social brain: ERP approaches for social cognitive and affective neuroscience. Soc. Cogn. Affect. Neurosci. 9, 385–393.

Amodio, D.M., Frith, C.D., 2006. Meeting of minds: the medial frontal cortex and social cognition. Nat. Rev. Neurosci. 7, 268–277.

Bault, N., Fahrenfort, J.J., Pelloux, B., Ridderinkhof, K.R., van Winden, F., 2017. An affective social tie mechanism: theory, evidence, and implications. J. Econ. Psychol. 61, 152–175.

Bellebaum, C., Kobza, S., Thiele, S., Daum, I., 2010. It was not MY fault: event-related brain potentials in active and observational learning from feedback. Cereb. Cortex. 20, 2874–2883.

Bilek, E., Zeidman, P., Kirsch, P., Tost, H., Meyer-Lindenberg, A., Friston, K., 2022. Directed coupling in multi-brain networks underlies generalized synchrony during social exchange. Neuroimage 252, 119038.

Billeke, P., Zamorano, F., Cosmelli, D., Aboitiz, F., 2013. Oscillatory brain activity correlates with risk perception and predicts social decisions. Cereb. Cortex. 23, 2872–2883.

Chen, M., Ma, Q., Li, M., Lai, H., Wang, X., Shu, L., 2010. Cognitive and emotional conflicts of counter-conformity choice in purchasing books online: an event-related potentials study. Biol. Psychol. 85, 437–445.

Chuang, T.M., Peng, P.C., Su, Y.K., Lin, S.H., Tseng, Y.L., 2024. Exploring inter-brain electroencephalogram patterns for social cognitive assessment during jigsaw puzzle solving. IEEE Trans. Neural Syst. Rehabil. Eng. 32, 422–430.

Clayson, P.E., Larson, M.J., 2013. Psychometric properties of conflict monitoring and conflict adaptation indices: response time and conflict N2 event-related potentials. Psychophysiology 50, 1209–1219.

Cohen, M.X., Elger, C.E., Ranganath, C., 2007. Reward expectation modulates feedback-related negativity and EEG spectra. Neuroimage 35, 968–978.

Du, X., Tang, Y., Jiang, Y., Tian, Y., 2022. Individuals attention bias in perceived loneliness: an ERP study. Brain-Appar. Commun.: J. Bacomics 1, 50–65.

Faul, F., Erdfelder, E., Lang, A.-G., Buchner, A., 2007. G* Power 3: a flexible statistical power analysis program for the social, behavioral, and biomedical sciences. Behav. Res. Methods 39, 175–191.

Fehr, E., Fischbacher, U., 2003. The nature of human altruism. Nature 425, 785–791.

Feldman, R., 2007. Parent-infant synchrony and the construction of shared timing; physiological precursors, developmental outcomes, and risk conditions. J. Child Psychol. Psychiatry 48, 329–354.

Gabay, A.S., Radua, J., Kempton, M.J., Mehta, M.A., 2014. The Ultimatum Game and the brain: a meta-analysis of neuroimaging studies. Neurosci. Biobehav. Rev. 47, 549–558.

Gehring, W.J., Willoughby, A.R., 2002. The medial frontal cortex and the rapid processing of monetary gains and losses. Science 295, 2279–2282.

Gonzalez, J.E., Nieto, N., Brusco, P., Gravano, A., Kamienkowski, J.E., 2024. Speech-induced suppression during natural dialogues. Commun. Biol. 7, 291.

Gouveia, V.V., Athayde, R., Gouveia, R., Gomes, A.I.A.S.d.B., Souza, R., 2010. Self-report altruism scale: evidences of construct validity. Aletheia 30–44.

Hassall, C.D., McDonald, C.G., Krigolson, O.E., 2019. Ready, set, explore! event-related potentials reveal the time-course of exploratory decisions. Brain Res. 1719, 183–193.

Hasson, U., Ghazanfar, A.A., Galantucci, B., Garrod, S., Keysers, C., 2012. Brain-to-brain coupling: a mechanism for creating and sharing a social world. Trends. Cogn. Sci. 16, 114–121.

He, T., Clifford, G., Tarassenko, L., 2006. Application of independent component analysis in removing artefacts from the electrocardiogram. Neural Comput. Appl. 15, 105–116.

Heffner, J., FeldmanHall, O., 2022. A probabilistic map of emotional experiences during competitive social interactions. Nat. Commun. 13, 1718.

Hillebrand, A., Tewarie, P., van Dellen, E., Yu, M., Carbo, E.W., Douw, L., Gouw, A.A., van Straaten, E.C., Stam, C.J., 2016. Direction of information flow in large-scale resting-state networks is frequency-dependent. Proc. Natl. Acad. Sci. USA 113, 3867–3872.

Jahng, J., Kralik, J.D., Hwang, D.U., Jeong, J., 2017. Neural dynamics of two players when using nonverbal cues to gauge intentions to cooperate during the Prisoner's Dilemma Game. Neuroimage 157, 263–274.

Jiang, J., Chen, C., Dai, B., Shi, G., Ding, G., Liu, L., Lu, C., 2015. Leader emergence through interpersonal neural synchronization. Proc. Natl. Acad. Sci. USA 112, 4274–4279.

Jiang, J., Dai, B., Peng, D., Zhu, C., Liu, L., Lu, C., 2012. Neural synchronization during face-to-face communication. J. Neurosci. 32, 16064–16069.

Jiang, K., Fujii, F., Shiinoki, T., 2019. Prediction of lung tumor motion using nonlinear autoregressive model with exogenous input. Phys. Med. Biol. 64, 21nt02.

Kayhan, E., Matthes, D., Marriott Haresign, I., Bánki, A., Michel, C., Langeloh, M., Wass, S., Hoehl, S., 2022. DEEP: a dual EEG pipeline for developmental hyperscanning studies. Dev. Cogn. Neurosci. 54, 101104.

Kingsbury, L., Hong, W., 2020. A multi-brain framework for social interaction. Trends. Neurosci. 43, 651–666.

Kingsbury, L., Huang, S., Wang, J., Gu, K., Golshani, P., Wu, Y.E., Hong, W., 2019. Correlated neural activity and encoding of behavior across brains of socially interacting animals. Cell 178, 429–446 e416.

König, N., Steber, S., Borowski, A., Bliem, H.R., Rossi, S., 2021. Neural processing of cognitive control in an emotionally neutral context in anxiety patients. Brain Sci. 11.

Larson, M.J., Clayson, P.E., Clawson, A., 2014. Making sense of all the conflict: a theoretical review and critique of conflict-related ERPs. Int. J. Psychophysiol. 93, 283–297.

Leong, V., Byrne, E., Clackson, K., Georgieva, S., Lam, S., Wass, S., 2017. Speaker gaze increases information coupling between infant and adult brains. Proc. Natl. Acad. Sci. USA 114, 13290–13295.

Li, R., Mayseless, N., Balters, S., Reiss, A.L., 2021. Dynamic inter-brain synchrony in real-life inter-personal cooperation: a functional near-infrared spectroscopy hyperscanning study. Neuroimage 238, 118263.

Luft, C.D.B., Zioga, I., Giannopoulos, A., Di Bona, G., Binetti, N., Civilini, A., Latora, V., Mareschal, I., 2022. Social synchronization of brain activity increases during eye-contact. Commun. Biol. 5, 412.

Ma, Y., Tan, H., 2023. Representation of intergroup conflict in the human brain. Neuron 111, 1692–1696.

Mayer, S.V., Rauss, K., Pourtois, G., Jusyte, A., Schönenberg, M., 2019. Behavioral and electrophysiological responses to fairness norm violations in antisocial offenders. Eur. Arch. Psychiatry Clin. Neurosci. 269, 731–740.

Mesrobian, S.K., Villa, A.E.P., Bader, M., Götte, L., Lintas, A., 2018. Event-related potentials during a gambling task in young adults with Attention-Deficit/ Hyperactivity disorder. Front. Hum. Neurosci. 12, 79.

Miraghaie, A.M., Pouretemad, H., Villa, A.E.P., Mazaheri, M.A., Khosrowabadi, R., Lintas, A., 2022. Electrophysiological markers of fairness and selfishness revealed by a combination of dictator and ultimatum games. Front. Syst. Neurosci. 16, 765720.

Ni, J., Yang, J., Ma, Y., 2024. Social bonding in groups of humans selectively increases inter-status information exchange and prefrontal neural synchronization. PLoS Biol. 22, e3002545.

Nieuwenhuis, S., Holroyd, C.B., Mol, N., Coles, M.G., 2004. Reinforcement-related brain potentials from medial frontal cortex: origins and functional significance. Neurosci. Biobehav. Rev. 28, 441–448.

Pan, Y., Vinding, M.C., Zhang, L., Lundqvist, D., Olsson, A., 2023. A brain-to-brain mechanism for social transmission of threat learning. Adv. Sci. 10, 2304037.

Paret, C., Ruf, M., Gerchen, M.F., Kluetsch, R., Demirakca, T., Jungkunz, M., Bertsch, K., Schmahl, C., Ende, G., 2016. fMRI neurofeedback of amygdala response to aversive stimuli enhances prefrontal-limbic brain connectivity. Neuroimage 125, 182–188.

Pfurtscheller, G., Lopes da Silva, F.H., 1999. Event-related EEG/MEG synchronization and desynchronization: basic principles. Clin. Neurophysiol. 110, 1842–1857.

Philippe Rushton, J., Chrisjohn, R.D., Cynthia Fekken, G., 1981. The altruistic personality and the self-report altruism scale. Pers. Individ. Dif. 2, 293–302.

Pick, H., Fahoum, N., Zoabi, D., Shamay Tsoory, S.G., 2024. Brainstorming: interbrain coupling in groups forms the basis of group creativity. Commun. Biol. 7, 911.

Pion-Tonachini, L., Kreutz-Delgado, K., Makeig, S., 2019. ICLabel: an automated electroencephalographic independent component classifier, dataset, and website. Neuroimage 198, 181–197.

Polezzi, D., Daum, I., Rubaltelli, E., Lotto, L., Civai, C., Sartori, G., Rumiati, R., 2008a. Mentalizing in economic decision-making. Behav. Brain Res. 190, 218–223.

Polezzi, D., Lotto, L., Daum, I., Sartori, G., Rumiati, R., 2008b. Predicting outcomes of decisions in the brain. Behav. Brain Res. 187, 116–122.

Qiao, X., Li, R., Huang, H., Hong, Y., Li, X., Li, Z., Chen, S., Yang, L., Ong, S., Yao, Y., Wang, F., Zhang, X., Lin, K.M., Xiao, Y., Weng, M., Zhang, J., 2025. Exploring the neural mechanisms underlying cooperation and competition behavior: insights from stereo-electroencephalography hyperscanning. iScience 28, 111506.

Rand, D.G., Tarnita, C.E., Ohtsuki, H., Nowak, M.A., 2013. Evolution of fairness in the one-shot anonymous Ultimatum Game. Proc. Natl. Acad. Sci. USA 110, 2581–2586.

Redcay, E., Schilbach, L., 2019. Using second-person neuroscience to elucidate the mechanisms of social interaction. Nat. Rev. Neurosci. 20, 495–505.

Rotter, J.B., 1967. A new scale for the measurement of interpersonal trust. J. Pers. 35, 651–665.

Rushworth, M.F., Noonan, M.P., Boorman, E.D., Walton, M.E., Behrens, T.E., 2011. Frontal cortex and reward-guided learning and decision-making. Neuron 70, 1054–1069.

Schippers, M.B., Roebroeck, A., Renken, R., Nanetti, L., Keysers, C., 2010. Mapping the information flow from one brain to another during gestural communication. Proc. Natl. Acad. Sci. USA 107, 9388–9393.

Speer, S.P.H., Mwilambwe-Tshilobo, L., Tsoi, L., Burns, S.M., Falk, E.B., Tamir, D.I., 2024. Hyperscanning shows friends explore and strangers converge in conversation. Nat. Commun. 15, 7781.

Szymanski, C., Pesquita, A., Brennan, A.A., Perdikis, D., Enns, J.T., Brick, T.R., Müller, V., Lindenberger, U., 2017. Teams on the same wavelength perform better: inter-brain phase synchronization constitutes a neural substrate for social facilitation. Neuroimage 152, 425–436.

Thielmann, I., Spadaro, G., Balliet, D., 2020. Personality and prosocial behavior: a theoretical framework and meta-analysis. Psychol. Bull. 146, 30–90.

Valencia, A.L., Froese, T., 2020. What binds us? Inter-brain neural synchronization and its implications for theories of human consciousness. Neurosci. Conscious. 2020, niaa010.

Vallet, W., Laflamme, V., Grondin, S., 2019. An EEG investigation of the mechanisms involved in the perception of time when expecting emotional stimuli. Biol. Psychol. 148, 107777.
van Dijk, E., De Dreu, C.K.W., 2021. Experimental games and social decision making. Annu. Rev. Psychol. 72, 415–438.
Whitehead, P.S., Brewer, G.A., Blais, C., 2017. ERP evidence for conflict in contingency learning. Psychophysiology. 54, 1031–1039.
Winkler, I., Haufe, S., Tangermann, M., 2011. Automatic classification of artifactual ICA-components for artifact removal in EEG signals. Behav. Brain Funct. 7, 30.
Yamagishi, T., Horita, Y., Mifune, N., Hashimoto, H., Li, Y., Shinada, M., Miura, A., Inukai, K., Takagishi, H., Simunovic, D., 2012. Rejection of unfair offers in the ultimatum game is no evidence of strong reciprocity. Proc. Natl. Acad. Sci. 109, 20364–20368.
Yang, J., Zhang, H., Ni, J., De Dreu, C.K.W., Ma, Y., 2020. Within-group synchronization in the prefrontal cortex associates with intergroup conflict. Nat. Neurosci. 23, 754–760.
Yao, D., 2001. A method to standardize a reference of scalp EEG recordings to a point at infinity. Physiol. Meas. 22, 693–711.
Yi, C., Yao, R., Song, L., Jiang, L., Si, Y., Li, P., Li, F., Yao, D., Zhang, Y., Xu, P., 2022. A novel method for constructing EEG large-scale cortical dynamical functional network connectivity (dFNC): WTCS. IEEE Trans. Cybern. 52, 12869–12881.
Yin, J., Yuan, K., Feng, D., Cheng, J., Li, Y., Cai, C., Bi, Y., Sha, S., Shen, X., Zhang, B., Xue, T., Qin, W., Yu, D., Lu, X., Tian, J., 2016. Inhibition control impairments in adolescent smokers: electrophysiological evidence from a Go/NoGo study. Brain ImAging Behav. 10, 497–505.
Zhang, D., Ao, X., Zheng, Z., Shen, J., Zhang, Y., Gu, R., 2022. Modulating social feedback processing by deep TMS targeting the medial prefrontal cortex: behavioral and electrophysiological manifestations. Neuroimage 250, 118967.
Zhang, D., Lin, Y., Jing, Y., Feng, C., Gu, R., 2019. The dynamics of belief updating in Human cooperation: findings from inter-brain ERP hyperscanning. Neuroimage 198, 1–12.
Zhang, H., Yang, J., Ni, J., De Dreu, C.K.W., Ma, Y., 2023. Leader–follower behavioural coordination and neural synchronization during intergroup conflict. Nat. Hum. Behav.
Zhang, W., Yartsev, M.M., 2019. Correlated neural activity across the brains of socially interacting bats. Cell 178, 413–428 e422.